Open Journal of Nano
ISSN: 2147-0081
(2022) 7–2
Research Article

Modification of PVDF Membranes Using Dopamine/Zinc Oxide Powders for Lead Removal from Aqueous Media

[1] İrem Sevim Üçel, [*1] Elif Demirel

[1] Eskisehir Technical University, Department of Chemical Engineering, Eskisehir/Turkey.
* Corresponding author, e-mail: elifyildiz@eskisehir.edu.tr, +90 222 3213550/6509

Submission Date: 15.01.2022 Acceptation Date: 21.03.2022

Abstract - Ultrafiltration (UF) has long been a leading separation technology with a strong historical track record for a wide range of applications such as the treatment of ground water, surface water and wastewater. The utilization of nanofillers in the fabrication of organic UF membranes has brought about breakthrough progress in membrane science and technology. The present study demonstrates modification of polyvinylidene fluoride (PVDF) membranes using zinc oxide (ZnO), polydopamine (PDA), and ZnO/PDA powders by blending and coating methods, respectively. ZnO/PDA nanoparticles were synthesized by the sol-gel method and were characterized using X-Ray Diffraction in comparison to ZnO and dopamine (DA) powders. Filtration performance of the fabricated membranes were determined in terms of water flux, sodium alginate (SA) rejection, and anti-fouling properties. Moreover, lead (Pb^{+2}) ions were chelated with chitosan following rejection of the formed lead-chitosan complexes from the fabricated membranes. Although water flux and SA rejections of the pristine PVDF membrane in the presence of different powders could not be substantially improved, anti-fouling properties could be enhanced markedly. PVDF/ZnO/PDA membrane was found to exhibit the best separation performance with 92% flux recovery ratio and 97% SA rejection and had the highest lead-chitosan removal of 88.5% from aqueous solutions. The enhanced separation performance of the PVDF/ZnO/PDA membrane was revealed by SEM images, which demonstrated remarkable morphological changes such as more porous, longer and interconnected finger-like formations compared with the pristine PVDF membrane.

Keywords: Membrane, Nanoparticle, Zinc Oxide, Dopamine, Lead removal

Sulu Ortamlardan Kurşun Giderimi için PVDF Membranların Çinko Oksit/Dopamin ile Modifiye Edilmesi

Öz - Ultrafiltrasyon (UF), uzun zamandır yeraltı suyu, yüzey suyu ve atık su arıtımı gibi çok çeşitli uygulamalarda kullanılan güçlü bir geçmişe sahip, lider bir ayırma teknolojisi olmuştur. Organik UF membranlarının üretiminde nano dolgu maddelerinin kullanılması, membran bilimi ve teknolojisinde çığır açan ilerlemeler sağlamıştır. Bu çalışmada, çinko oksit (ZnO), polidopamin (PDA) ve ZnO/PDA tozları sırasıyla harmanlama ve kaplama yöntemleri ile poliviniliden florür (PVDF) membranlarının modifikasyonu için kullanılmıştır. ZnO/PDA nanoparçacıkları sol-jel yöntemi ile sentezlendikten sonra, X-Işını Kırınım ile ZnO ve dopamin (DA) tozları ile karşılaştırılarak karakterize edilmiştir. Üretilen membranların filtrasyon performansı, su akısı, sodyum aljinat (SA) giderimi ve kirlenmeye karşı direnç özellikleri ile belirlenmiştir. Ayrıca, kurşun (Pb^{+2}) iyonlarının kitosan ile kompleks haline getirilmesinden sonra oluşan kurşun-kitosan komplekslerinin membranlardan giderimi test edilmiştir. Saf PVDF membranın su akısı ve SA giderimi farklı tozlar varlığında kayda değer bir miktarda arttırılamasa da, kirlenmeye karşı direnç özellikleri önemli ölçüde iyileştirilmiştir. PVDF/ZnO/PDA memranının %92 su akısı geri kazanım oranı ve %97 SA giderimi ile en iyi ayırma performansı gösterdiği ve sulu çözeltilerden en yüksek kurşun-kitosan giderimini (%88,5) sağladığı belirlenmiştir. PVDF/ZnO/PDA membranının iyileştirilmiş ayırma performası, saf PVDF membrana kıyasla daha gözenekli, uzun ve birbirine bağlı parmaksı oluşumların varlığını gösteren SEM görüntüleri ile ortaya koyulmuştur.

Anahtar kelimeler: Membran, Nanotanecik, Çinko Oksit, Dopamin, Kurşun giderimi

[1] Corresponding author: Tel: +90 222 3213550/6509

E-mail: elifyildiz@eskisehir.edu.tr,

Open Journal of Nano
ISSN: 2147-0081
(2022) 7–2
Research Article

1. Introduction

In recent years, the limited availability of freshwater, which plays an important role in human life and the ecosystem, has led to a great interest in water and wastewater treatment technologies [1]. Surface and groundwater pollution, which has become a global environmental problem due to rapid population growth and global industries reveals the importance of wastewater treatment [1,2,3]. Besides, wastewater treatment is an important issue that needs to be addressed, as only 0.5% of the water in the world is fresh water [4,5]. The release of heavy metal ions, which are toxic even at low levels and cause damage to human health and the aquatic ecosystem, into water sources without adequate treatment is one of the main causes of surface and groundwater pollution [1,6,7,8]. In particular, heavy metals such as arsenic, cadmium, and lead must be removed from wastewater before they accumulate in living organisms. These non-biodegradable heavy metals have become an issue of great concern due to their hazardous effects. Especially lead is one of the most toxic metal pollutants and lead pollution has become an issue of great concern due to its large discharge and high mobility in an aqueous environment, and easy accumulation in the human body. Lead exposure is known to damage the nervous system, kidneys, and reproductive system, and excessive lead exposure can lead to headaches, stomach pain, cancer, and even death. Therefore, The World Health Organization (WHO) ascribes lead as one of the greatest public health issues [8,9,10,11]. According to WHO, the maximum contaminant level (MCL) of Pb^{+2} in drinking water should be less than 15 µg/L [12].

Many technologies such as chemical precipitation, coagulation-flocculation, adsorption, membrane technology, ion exchange, and electrochemical purification are applied in the separation of lead from water [9]. In the last decades, membrane separation processes have become widespread owing to a number of advantages including high efficiency, easy integration with other separation techniques, feasible scale-up, and improvable fabrication techniques [13,14]. The most common membrane processes particularly applied for water treatment are microfiltration (MF), ultrafiltration (UF), nanofiltration (NF), reverse osmosis (RO), electrodialysis, and membrane distillation. NF and RO membranes are used in various water treatment processes and heavy metal removal due to their appropriate pore sizes, but they require higher pressure and energy consumption compared to UF and MF processes. However, the application of UF and MF processes for the removal of heavy metals is limited due to their large pore structure. Therefore, modification of UF/MF membranes is necessary to enable the removal of heavy metal ions from aqueous solutions [11]. Membrane fouling, which is the most limiting factor for wider applications of membrane processes, causes a serious reduction in permeability and considerable technical problems such as requirement for higher operating pressures and harsh cleaning conditions [6,11,15]. The incorporation of fillers into the membrane matrix by physical blending, chemical grafting, and surface modifications has been demonstrated to enhance the hydrophilicity, permeability, and contamination resistance of the membrane [16, 17]. Zinc oxide (ZnO) has been used as a membrane filler for its exceptional physical and chemical properties as well as its antibacterial activity [16,18]. Dopamine (DA), which is a very hydrophilic molecule and biocompatible with catechol and amino groups, has recently attracted considerable attention in the modification of membranes. DA is a highly suitable material for surface modification since it self-polymerizes to polydopamine (PDA) under alkaline conditions on almost any surface regardless of its morphology or chemical composition [19, 20, 21]. PDA coating has several advantages such as electrostatic attraction, chelation, and covalent bonds with the surface [21]. Some studies on the synthesis of ZnO/PDA powders and their incorporation into membrane matrix with an aim to enhance filtration performance have been reported in the literature. Tavakoli et al. synthesized a new composite material by decorating ZnO nanoparticles with PDA and reported that the oxygen atoms in the ZnO were bonded to hydrogen atoms in the amine and catechol functional groups of the PDA molecule through hydrogen intermolecular forces. They also reported that coating ZnO nanoparticles

Open Journal of Nano
ISSN: 2147-0081
(2022) 7–2
Research Article

with PDA did not result in a change in their morphology, but some spherical precipitations on the surface of the nanoparticles confirmed the presence of PDA coating [22]. Zhang et al. incorporated PDA-modified titanium dioxide (TiO_2) fillers into the PVDF membrane matrix by blending method and also coated the membrane surface with PDA and reported that water flux of pristine PVDF membrane increased by 312% and 287% by coating the membrane using 2 g/L DA solution and with the addition of a PDA-modified TiO_2 additive by blending method, respectively [20].

In addition to the membrane modification methods mentioned above such as incorporation of fillers into the membrane matrix by physical blending, chemical grafting, and surface modifications, the complexation–membrane filtration or polymer-assisted ultrafiltration (PEUF) is another noteworthy technique for heavy metal removal from water [23]. The overall idea of this method is based on binding the cationic heavy metals to a water-soluble polymer to increase the molecular weight of the heavy metal so as to retain even trace amounts of metal on the membrane surface [23, 24]. The use of polymers containing carboxylic or amine groups as complexing agents such as carboxyl methylcellulose (CMC) [25], polyvinylethylenimin (PEI) [26,27], polyvinyl alcohol (PVA) [27], poly(acrylic acid) (PAA) [28], and chitosan have been reported to be capable of removing several heavy metals from wastewater. Chitosan is a natural biodegradable polymer that can be used to bind metal ions by interacting with them through -OH and -NH_2 functional groups. That is, the stoichiometry of chitosan-metal complex is based on the number of amine groups (R-NH_2) bound to the metal ions [29]. The formation of probable metal-chitosan complex is given in Figure 1. Metal-complexing agent ratio and pH of the solution are significant parameters that affect the removal efficiency of the metal, while membrane characteristics and operating conditions of the process influence the reusability of the membrane. Polymer can easily be removed from the complex subsequent to filtration.

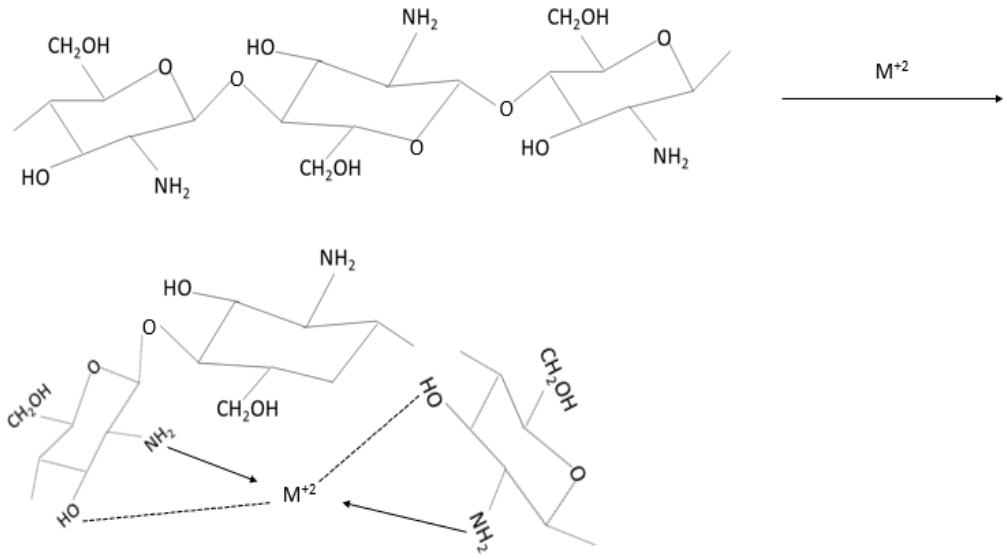

Figure 1. Probable molecular structure of the metal (M^{+2})-chitosan complex.

Although several studies have attempted to incorporate different fillers including ZnO, DA, PDA along with their combined forms into polymer-based membrane matrices, utilizing them for heavy metal removal from aqueous media using polymer assisted ultrafiltration technique is still lacking in the literature. Present study aims at fabricating polyvinylidene fluoride (PVDF) based nanocomposite membranes modified with ZnO, PDA, and ZnO/PDA powders using the phase inversion technique for the investigation of their separation performance not only in terms of lead removal from aqueous solutions but also other filtration characteristics such as water flux and anti-fouling properties in

Open Journal of Nano
ISSN: 2147-0081
(2022) 7–2
Research Article

comparison to that of pristine PVDF membrane. In this context, ZnO and ZnO/PDA powders were incorporated into the membrane matrix in certain proportions by blending method, and PDA was added by coating method. Membrane characterization was carried out by exploring their morphology, porosity, mean pore size, bulk thermal stability, and mechanical strength using several equipments and analytical techniques. In addition, as a complexing agent, chitosan was employed in polymer-assisted ultrafiltration process to remove lead ions from aqueous solutions and the highest lead-chitosan removal performance was highlighted by investigating the main operating conditions such as lead: chitosan ratio and pH of the solution.

2. Materials and Methods

2.1. Chemicals

PVDF (Molecular Weight (MW) = 534,000 $g.mol^{-1}$), polyethylene glycol (PEG, MW= 6,000 Da), 3,4-dihydroxyphenethylamine (dopamine hydrochloride), Tris(hydroxymethyl) aminomethane (Tris), ZnO (particle size <100 nm), chitosan (from shrimp shells, ≥75%) and sodium alginate (SA) were purchased from Sigma-Aldrich. 1-Methyl-2-pyrrolidone (NMP, >99%) and lead nitrate ($PbNO_3$) were supplied by Alfa Aesar and Carlo Elba, respectively. All the other chemicals were used as received without further treatment. Deionized (DI) water was produced by a Milli-Q system (Millipore, US).

2.2. Synthesis of ZnO/PDA Powders

ZnO/PDA nanoparticles were prepared by the sol-gel method using ZnO and dopamine hydrochloride (DA) [20]. 0.5 g ZnO nanoparticle was added into 50 mL DI water and ultrasonically dispersed for 30 min. Besides, a Tris solution with a concentration of 1.0 g/L was prepared and its pH was adjusted to 8.5 using either NaOH or HNO_3 solutions. 0.5 g DA was ultrasonically dispersed in 200 mL Tris-HCl buffer. PDA solution was obtained by self-polymerization of dopamine in tris-HCl buffer solution since hydrophilic DA can self-polymerize under alkaline conditions. The ZnO suspension prepared in the first step and DA solution were mixed in a magnetic stirrer at room temperature for 24 h. The sediment obtained was centrifuged at 5000 rpm and then filtered under vacuum. Finally, the ZnO/PDA nanoparticles were washed with ethyl alcohol and DI water three times and then dried at 85 °C prior to characterization.

2.3. Fabrication of Membranes

Pristine PVDF, ZnO, and ZnO/PDA doped nanocomposite membranes were fabricated using blending and phase inversion with immersion precipitation technique [20]. For the preparation of membrane casting solutions, ZnO or ZnO/PDA nanoparticles (0.5wt. % of PVDF) were added into NMP and stirred in an ultrasonic bath for 3 and 1 hours, respectively. After the addition of PVDF and PEG, the resulting mixture was stirred at 70°C for 48 hours to get a homogenous solution. The casting solution was poured on a glass plate and cast into a film of 150 μm thickness using an adjustable casting blade and the thin film was immediately immersed into a coagulation bath of nonsolvent water. Membrane was transferred into a container of fresh water to get rid of the residual NMP. All the membranes were dried in an oven at 50°C under vaccum for 24 hours before the characterization tests [20]. The viscosity of each casting solution was measured at least twice using a Rotational Viscometer (Fungilab, Smart R, Spain) at room temperature with 50 rpm speed and 60% torque, and the average values are reported [30].

To investigate the effect of PDA coating, a pristine PVDF membrane was immersed into a 2 g/L DA solution for 24 hours. For this purpose, 0.4 g DA was added into 200 mL ethanol-Tris-HCl buffer solution (1:1, v/v) and the pH was adjusted to 8.5. The solution was stirred at 25°C for 24 hours, and the DA in the solution was self-polymerized into PDA [31]. Finally, nanocomposite membranes were washed with DI water and ethanol to remove the residual PDA particles [32].

Open Journal of Nano
ISSN: 2147-0081
(2022) 7–2
Research Article

The compositions of the membranes prepared by blending and coating methods are listed in Table 1.

Table 1. The compositions and viscosities of the casting solutions.

Membran ID	PVDF (g)	PEG (g)	NMP (g)	Additives (%wt.)	Viscosity (Pa.s)
PVDF	9	0.5	40.500	-	9.7
PVDF/ZnO	9	0.5	40.455	0.5 ZnO	10.8
PVDF/ZnO/PDA	9	0.5	40.455	0.5 ZnO/PDA	14.6
PVDF/PDA	9	0.5	40.455	PDA	-

2.4. Characterization

The morphology of the top surface and cross-section of the pristine and nanocomposite membranes were determined by Field Emission-Scanning Electron Microscopy (FE-SEM) (Hitachi Regulus 8230).

Membrane porosity was calculated by gravimetric method using the following equation [33].

$$\varepsilon = \frac{W_w - W_d}{\rho_w(\pi r^2 l)} \times 100\% \quad (1)$$

where W_w and W_d are the masses of the wet and dry membranes (g), respectively, ρ_w is the density of the water at room temperature (g/cm^3), r is the radius (cm), and l is the thickness (cm) of the membrane.

The mean pore diameter of the membrane was calculated using the Guerout-Elford-Ferry equation given below [34, 35].

$$a = \sqrt{\frac{(2.9 - 1.75\varepsilon) * (8\mu l Q_w)}{\varepsilon A \Delta P}} \quad (2)$$

where a denotes the mean pore diameter (m), ε is the porosity, μ is the viscosity of the filtrated water at room temperature (Pa.s), Q_w is the water flux (m^3/s), l is the thickness (m), A is the filtration area of the membrane (m^2), and ΔP is the transmembrane pressure (Pa).

The crystallinity of ZnO, DA, ZnO/PDA powders, and the fabricated membranes nanocomposite membranes were characterized by X-ray diffraction (XRD) analysis (Rigaku Miniflex 600). The addition of ZnO and ZnO/PDA fillers and the effect of PDA coating on the thermal behavior of the pristine membrane were investigated by thermogravimetric analysis (TGA, Perkin Elmer (STA) 6000). The functional groups of pristine and nanocomposite membranes were characterized by Fourier-Transform Infrared Spectroscopy (FTIR) (Thermofisher Science, Nicolet iS10). The mechanical stabilities of the membranes were determined using a single-column mechanical tensile tester (Instron 5944) and the results are reported in terms of Young modulus (MPa), tensile strength (MPa), and elongation at break (%).

2.5. Separation Performance of Membranes

Water flux values of the membranes were measured using a dead-end ultrafiltration system. A membrane sample with an effective surface area of 28.7 cm^2 was placed in a stirred cell (Millipore, Amicon Stirred Cell) of 200 mL capacity. Each membrane was compacted at 0.21 MPa for 1 h before

Open Journal of Nano
ISSN: 2147-0081
(2022) 7–2
Research Article

the ultrafiltration experiments. Then the pressure was lowered to 0.07 MPa and all the ultrafiltration experiments were carried out at this transmembrane pressure (TMP). The solution in the cell was stirred at 400 rpm to minimize concentration polarization [33]. Permeate was weighed in one-minute time intervals using a balance, and the data was collected and stored using a software (Radwag, Poland). The water flux was calculated using the following equation.

$$J_{w,1} = \frac{\Delta V}{A * \Delta t} \tag{3}$$

where $J_{w,1}$ is the pure water flux (L/m^{2}h), ΔV is the volume change of the permeate (L) in one-minute time interval, A is the membrane filtration area (m^2), and Δt is the permeation time (h).

The water flux values of the membranes were determined at different TMP (0.07-0.27 MPa) to investigate the compaction behavior and stability of membranes.

Rejection tests of the fabricated membranes were carried out using SA solution with a concentration of 20 mg/L. Concentrations of the collected permeate and feed for each membrane were determined quantitatively using a TOC-L Analyzer (Shimadzu, Japan) and calculated by the following equation [33].

$$R(\%) = \left(1 - \frac{C_P}{C_f}\right) \times 100 \tag{4}$$

where C_p and C_f are the concentrations of the permeate and feed solutions, respectively.

To assess the anti-fouling properties, a membrane sample was subjected to SA solution for 4 hours, washed with DI water and the flux was measured again. The anti-fouling property was interpreted in terms of flux recovery ratio (FRR), which was calculated using the equation below [36].

$$FRR\ (\%) = \frac{J_{w,2}}{J_{w,1}} \times 100 \tag{5}$$

where $J_{w,1}$ and $J_{w,2}$ denote the pure water flux and water flux after the SA fouling test, respectively.

During SA filtration, foulant molecules are adsorbed on the surface and inside fingerlike pores of the membrane structure that in turn leads to a flux decline. To understand the fouling resistances of the membranes, the resistance-in-series model was used [17, 36].

$$R_t = R_m + R_r + R_{ir} = \frac{\Delta P}{\mu * J_{W,2}} \tag{6}$$

where R_t denote the total fouling resistance of the membrane (m^{-1}), (R_m) is the intrinsic membrane resistance (m^{-1}), R_{ir} is the irreversible fouling resistance (m^{-1}), R_r is the reversible fouling resistance (m^{-1}), $J_{w,2}$ is the water flux after the SA fouling test (m^3/m^2.s), ΔP is the corresponding transmembrane pressure in (Pa) and μ is the dynamic viscosity of water at room temperature (Pa.s) [17]. Each resistance was computed using the following equations.

Open Journal of Nano
ISSN: 2147-0081
(2022) 7–2
Research Article

$$R_m = \frac{\Delta P}{\mu * J_{w,1}} \quad (7)$$

$$R_r = \frac{\Delta P}{\mu * J_{w,3}} - R_m \quad (8)$$

$$R_{ir} = R_t - R_m - R_r \quad (9)$$

where $J_{w,3}$ denotes the pure water flux ($m^3/m^2.s$) measured after backwashing of membranes for 30 min.

2.6. Lead Removal Efficiency

The performance of the fabricated membranes was tested for Pb^{+2} removal from aqueous solutions using polymer assisted ultrafiltration method. For this purpose, Pb^{+2} ions were bound to chitosan to form a lead-chitosan complex before the filtration experiments [29, 37]. For this purpose, 10 ppm Pb^{+2} solution was added to chitosan solutions of different concentrations (500 ppm and 1000 ppm) in 0.4 vol% acetic acid, and the resulting mixture is stirred for 24 hours to form a complex. pH was adjusted to the desired value using either 0.1 M NaOH or 0.1 M HNO_3 solutions. The concentrations of the permeate and the feed were determined using UV-Vis Spectrophotometer (Shimadzu, UV 2600/2700) at a wavelength of 200 nm.

3. Results and Discussions

3.1. Characterization of Nanoparticles

The crystallinity of ZnO, DA, and ZnO/PDA powders was characterized by XRD analysis. As shown in Figure 2a, the peaks observed at 31.82°, 34.46°, 36.3° corresponded to the hexagonal wurtzite crystal structure of ZnO [22, 38, 39, 40]. The peaks observed at 23.1°, 25.9°, 26.7°, 27.7°, 28.7°, and 31.3° in Fig. 2b were attributed to the characteristic peaks of DA that confirmed its crystalline structure [41]. XRD pattern of ZnO/PDA (Fig. 2c) powder had diffraction peaks similar to those of ZnO nanoparticles indicating that PDA did not cause any destruction during its interaction with ZnO and the crystalline structure of DA was degraded due to its self-polymerization into PDA [22, 41].

3.2. Effects of Environmental Conditions on Adsorption Study

The surface and cross-section images of the pristine and nanocomposite membranes were determined by SEM analysis and the results are given in Figure 3 and Figure 4, respectively. As shown in Figure 3, the pristine PVDF membrane exhibited the largest surface porosity with some defects and nonuniform distribution of pores and the number of the surface pores decreased with the addition of nanoparticles into the membrane matrix. A significant amount of ZnO clusters (as highlighted with yellow circles in Fig. 3b) were observed on the surface of the PVDF/ZnO membrane, indicating that ZnO was not uniformly distributed in the matrix due to its poor interaction with PVDF [42]. However, the incorporation of functional ZnO/PDA powders to the membrane matrix enhanced the interaction of PDA chains with PVDF, which in turn led to a uniform distribution surface pores in the matrix. As also shown in Figure 3c, negligible amount of aggregates (shown with yellow circles in Fig. 3c) were detected on the membrane surface. PVDF/PDA membrane had the lowest porosity with a significant amount of PDA clusters on the coating surface (shown with yellow circles in Fig. 3d) [43].

Open Journal of Nano
ISSN: 2147-0081
(2022) 7–2
Research Article

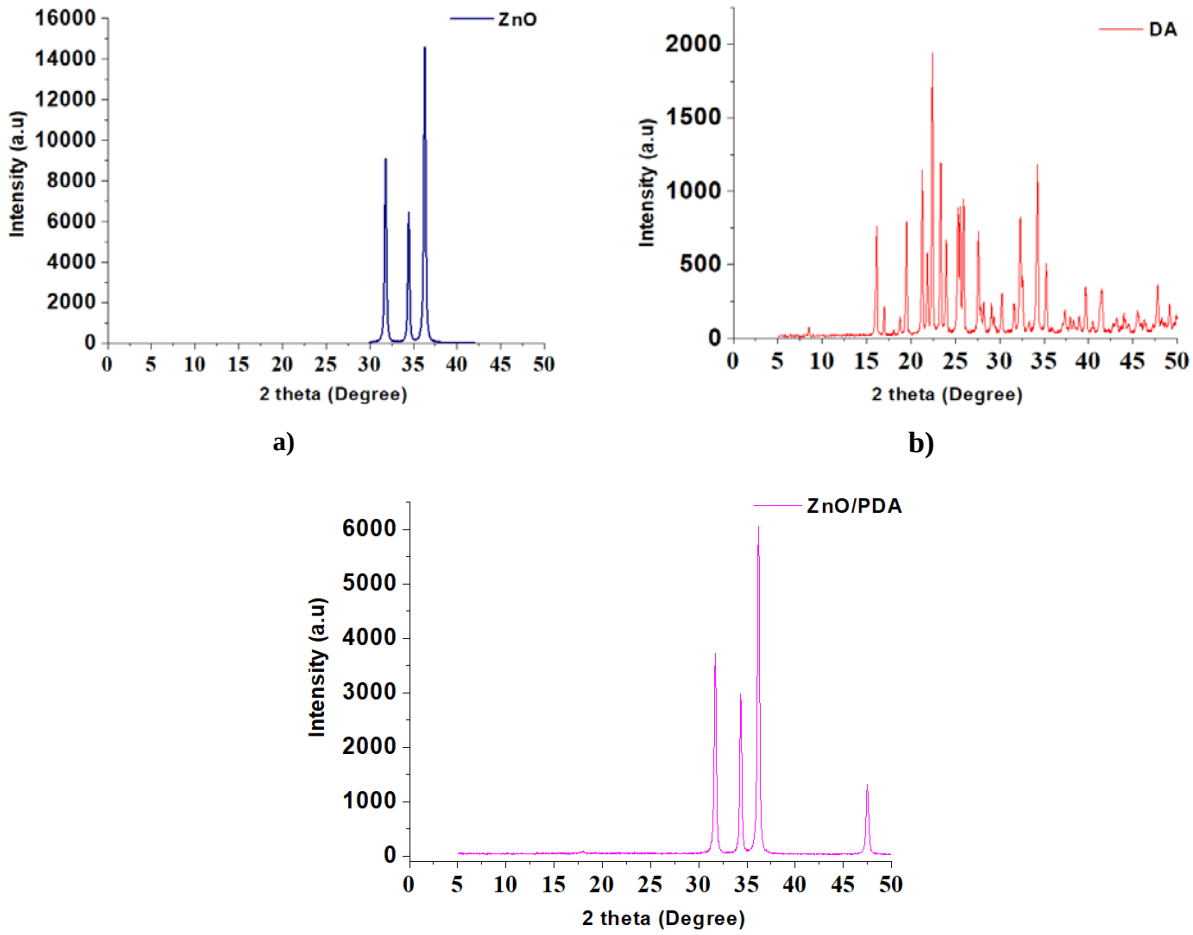

Figure 2. XRD patterns of nanoparticles a) ZnO b) DA c) ZnO/PDA.

As seen in Figure 4, all membranes consisted of an active upper layer with a low pore density and a support layer containing larger macropores, where the active upper layer separated by an orange line from the support layer [13,44]. The finger-like structures (yellow circles in Fig. 4) of the pristine PVDF membrane extended along the membrane cross-section. However, with the addition of ZnO to the matrix, as the size of the finger-like pore sizes were shortened, macroporous gaps (red circles in Fig.4b) occurred in the lower sections. However, PVDF/ZnO/PDA membrane showed finger-like formations, which extended along the cross-section, similar to that of the pristine PVDF membrane. Due to the non-uniform distribution of PDA powders on the coating surface, apparently the finger-like pores in the cross-section of the PVDF/PDA membrane was almost eliminated, and instead macroporous gaps (red circles in Fig.4d) were formed at the membrane base.

Some morphological properties of the fabricated membranes are given in Table 2. The porosity and mean pore diameter of the PVDF/ZnO nanocomposite membrane (84.6% and 14.1 nm, respectively) were similar to those of the pristine PVDF membrane (85.4% and 14.4 nm, respectively) since ZnO nanoparticles could not be distributed evenly over the membrane surface and finger-like pores (Table 2). The PVDF/ZnO/PDA membrane had the highest porosity (96.1%) with a comparatively smaller mean pore size indicating the existence of a large number of smaller pores in the matrix. The mean pore diameter (10.5 nm) of the PVDF/PDA membrane was the lowest since a long coating time may have caused the formation of a thick PDA layer on the surface or probably PDA aggregates clogged the membrane pores [45]. The morphological properties of membranes were in good agreement with the water permeability values.

Open Journal of Nano
ISSN: 2147-0081
(2022) 7–2
Research Article

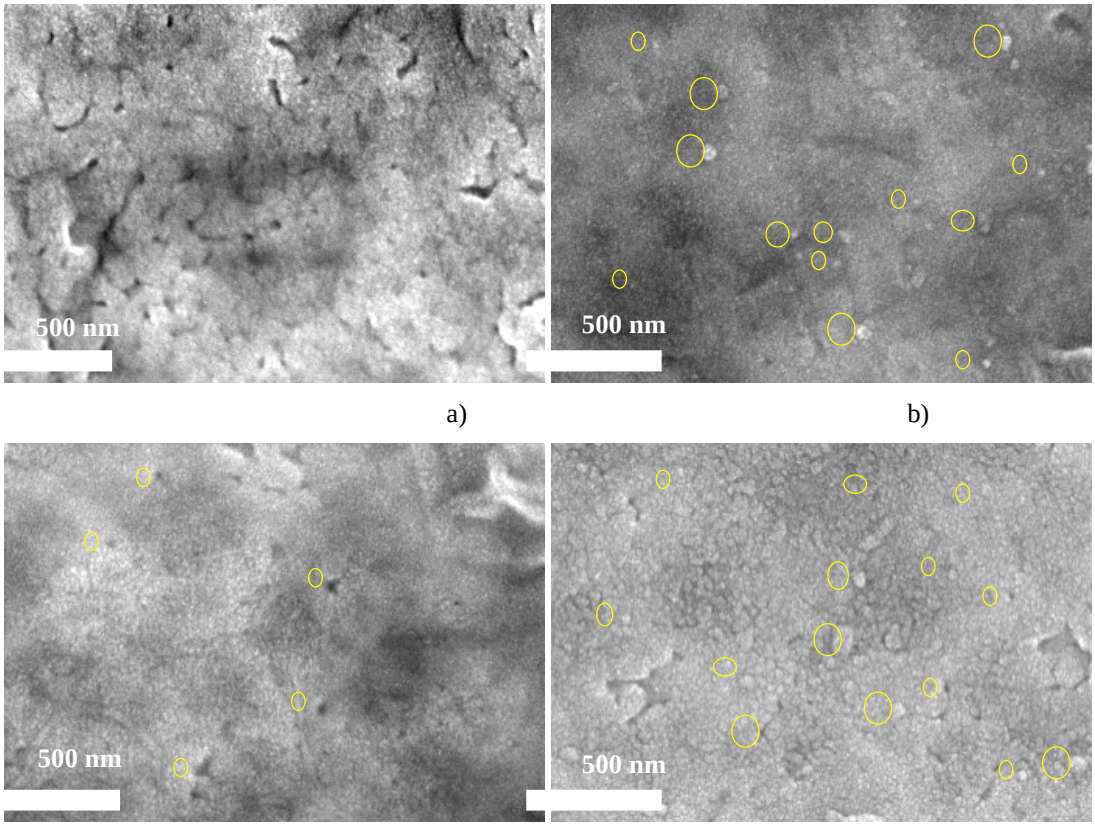

Figure 3. Surface SEM images of the membranes a) PVDF b) PVDF/ZnO c) PVDF/ZnO/PDA d) PVDF/PDA.

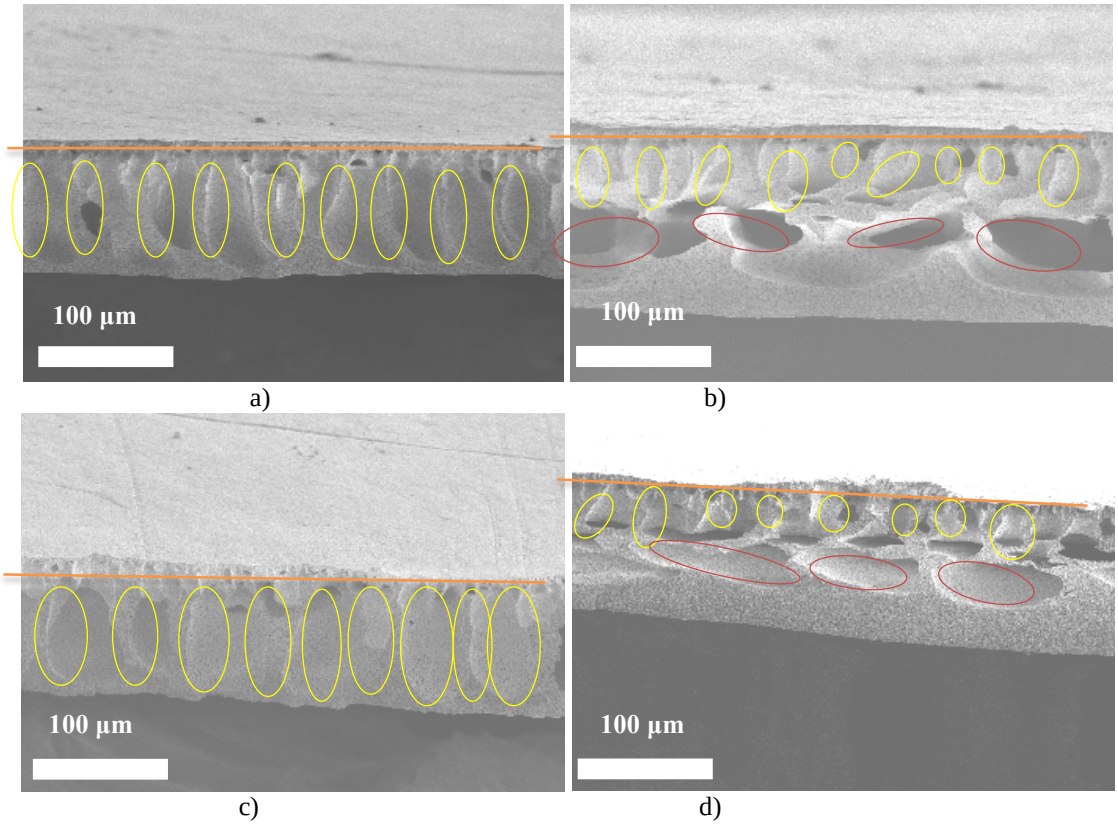

Figure 4. Cross-section SEM images of the membranes a) PVDF b) PVDF/ZnO c) PVDF/ZnO/PDA d) PVDF/PDA.

Open Journal of Nano
ISSN: 2147-0081
(2022) 7-2
Research Article

Table 2. Some morphological properties of membranes.

Membran ID	Porosity (%)	Mean pore diameter (nm)	Thickness (µm)
PVDF	85.4	14.4±0.8	73±2
PVDF/ZnO	84.6	14.1±0.5	77±2
PVDF/ZnO/PDA	96.1	12.8±0.4	75±2
PVDF/PDA	93.3	10.5±0.5	74±2

The crystallinity of the pristine PVDF membrane and nanocomposite membranes were characterized by XRD analysis. It can be seen from Figure 5 that, the characteristic diffraction peaks of the PVDF membrane observed at 18.8°, 21.1°, and 39°correspond to (020) (110) and (131) planes of the PVDF polymer. The fact that the peak intensity increased in Figure 5b could be attributed to the non-uniform distribution of ZnO nanoparticles in the membrane matrix [46]. The XRD patterns of PVDF/ZnO/PDA and PVDF/PDA membranes were similar to that of pristine PVDF membrane with no significant changes in the crystal structure [47, 48].

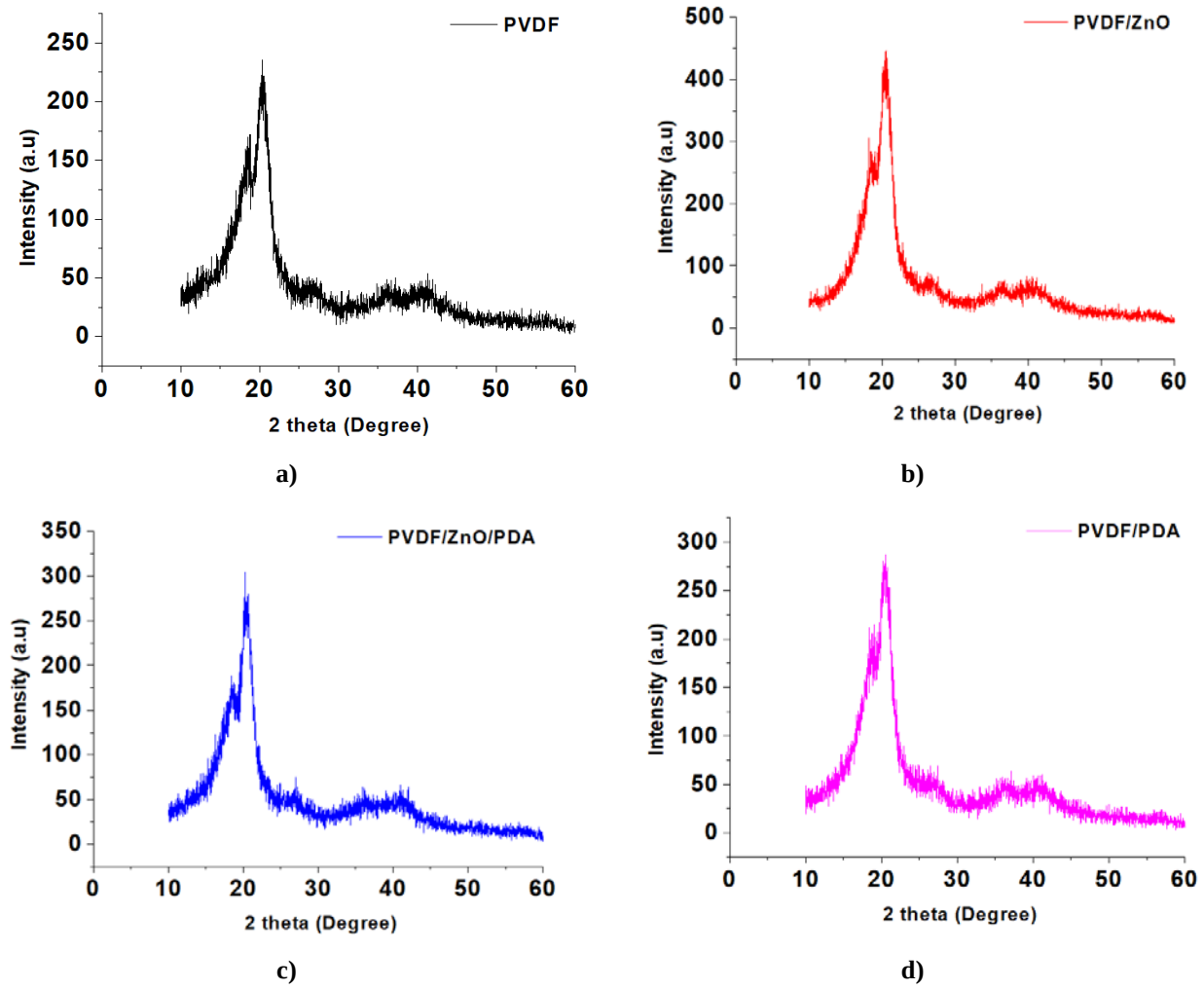

Figure 5. XRD patterns of membranes a) PVDF b) PVDF/ZnO c) PVDF/ZnO/PDA d) PVDF/PDA.

Functional groups of all membranes determined by FTIR analysis are given in Figure 6. The spectra of PVDF/ZnO and PVDF/ZnO/PDA nanocomposite membranes are quite similar. The wide peaks between 3500 cm^{-1} and 2950 cm^{-1} could correspond to the stretching vibrations of the N-H and hydroxyl groups resulting from catechol, which is the main functional group of PDA. The bands at 3500 cm^{-1} were assigned to the O-H group of adsorbed water [38]. In addition, new clear peaks at 1500-1700 cm^{-1} in the spectra of PVDF/PDA/ZnO and PVDF/PDA membranes were attributed to the

Open Journal of Nano
ISSN: 2147-0081
(2022) 7-2
Research Article

superposition of phenylic C-C stretching vibrations, N-H bending vibrations, and N-H shearing vibrations [49]. The FTIR spectra of the membranes show vibrational peaks at about 840 and 700 cm^{-1}, which are typical vibrational characteristics of the β-crystal phase [50]. The bands at 1177, 977, 840, and 509 cm^{-1} are able to be assigned to the vibration of the β-PVDF polymorphic phase [51]. It was observed that the intensity of the bands at 1177 and 840 cm^{-1} increased after the addition of ZnO nanoparticles which indicated that ZnO nanoparticles enhanced the crystallization of the β-PVDF phase. In addition, the strong absorption band at 1177 cm^{-1} is able to associate with the stretching vibration of $–CF_2$ [51].

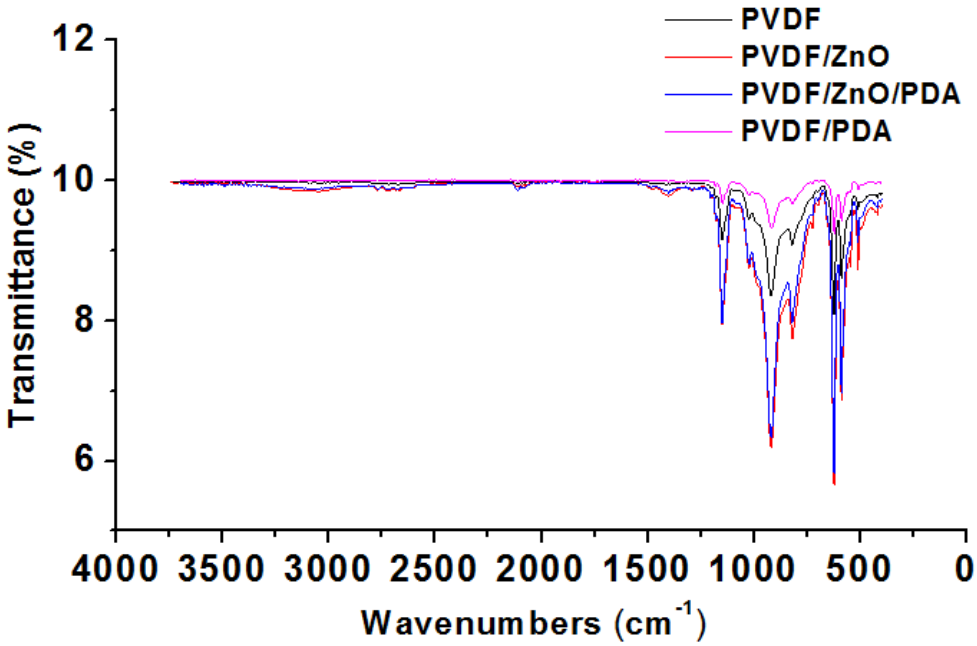

Figure 6. FTIR spectra of the pristine PVDF and modified nanocomposite membranes.

The thermal properties of the fabricated membranes investigated using TGA analysis are given in Figure 7. The degradation of the pristine membrane occurred between 430-500°C with a mass loss of 65%. Decomposition temperatures of ZnO-doped and the PDA-coated composite membranes were similar to that of the pristine PVDF membrane, which was probably due to the fact that neither the ZnO nanoparticles and nor the PDA layer could not be distributed homogeneously in the polymer matrix, as also supported by SEM analyses results. Decomposition of the PVDF/ZnO/PDA nanocomposite membrane was observed in the range of 470-510°C with a mass loss of 57%. This improvement in thermal stability of PVDF/ZnO/PDA membrane could be attributed to the strong interaction of ZnO/PDA powders with the polymer chains [21, 31].

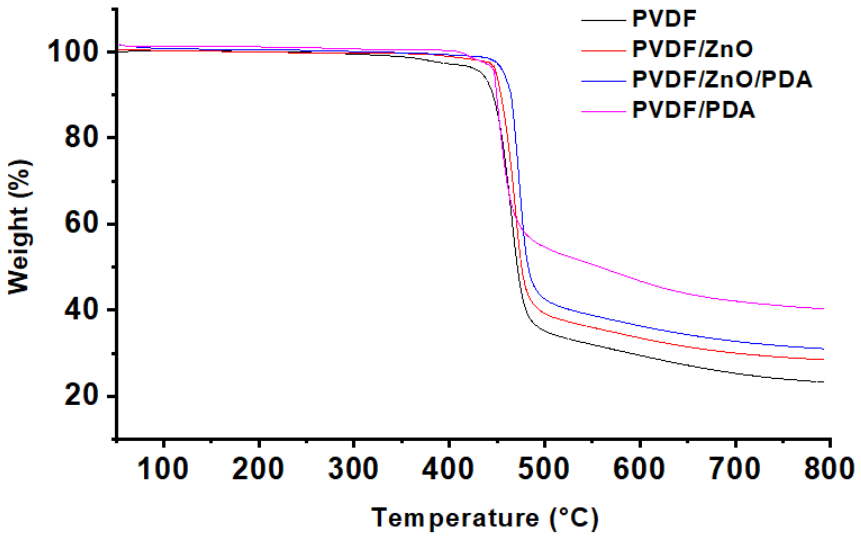

Open Journal of Nano
ISSN: 2147-0081
(2022) 7–2
Research Article

Figure 7. TGA thermograms of the fabricated membranes.

Mechanical properties of the pristine PVDF and nanocomposite membranes were evaluated by Young's modulus (MPa), tensile strength (MPa), and elongation at break (%), and the results are presented in Table 3. The mechanical properties of porous membranes depend mainly on the characteristics of the polymer, fillers as well as porosity and pore size distribution of porous membranes. The Young's modulus, which is a measure of stiffness of a material, can be found from the slope of the stress-strain curve in the elastic region, which describes how much of the material tested deforms for different levels of applied stress. As shown in Table 3, the Young's modulus of the pristine PVDF membrane was 67.1 MPa and increased to 117.8 MPa and 98.9 MPa with the addition of ZnO and ZnO/PDA powders to the membrane matrix, respectively. A more rigid structure of both composite membranes could be attributed to the presence of nanofillers serving as a bridge between the polymer chains [52]. Tensile strength is the value of the maximum stress that a material can handle. The tensile strength of the PVDF/ZnO and PVDF/ZnO/PDA membranes had higher values in comparison to that of pristine PVDF membrane since more energy would be required to break the bonds between ZnO and PVDF and also between PDA/ZnO and PVDF due to the rigidity enhancement of polymer chains [18]. The elongation at the break is an indicator of the elasticity of a material. Elongation at break of the PVDF membrane increased from 14.5% to 19.0% with the addition of ZnO/PDA powders into the membrane matrix since PDA was able to absorb energy during the tensile test, thereby leading to a decrease in the fragility of the membranes [49, 53]. However, even though PVDF/ZnO membrane exhibited the highest Young's modulus and tensile strength values, significant amount of ZnO clusters observed on the PVDF/ZnO membrane surface (Figure 3b) led to weaker interactions of the nanoparticles with the polymer chains in some spots and resulted a decrease in the rupture elongation value of the membrane [54]. It is well known that nanoparticles can significantly resist the applied stress and improve the modulus on the condition that they are uniformly distributed along the matrix. Any defects resulted from aggregations can remarkably reduce the mechanical strength due to brittleness [55]. Although the mechanical properties are expected to be better for membranes with a smaller pore size, due to the non-uniform distribution of PDA fillers on the surface caused the formation of weak stress zones, which in turn resulted in the poor mechanical stability of the PVDF/PDA membrane [56]. However, when the PVDF/ZnO/PDA membrane is examined, it is seen that the mechanical properties of the membrane improve as an effect of the distribution of ZnO/PDA powders in the membrane matrix.

Table 3. Mechanical properties of the membranes.

Membrane ID	Young's modulus (MPa)	Tensile strength (MPa)	Elongation at break (%)
PVDF	67.1±1.85	1.89±0.35	14.5±2.88
PVDF/ZnO	117.8±4.02	2.23±0.49	10.4±0.57
PVDF/ZnO/PDA	98.9±3.05	2.15±0.43	19.0±2.00
PVDF/PDA	61.9±2.87	1.69±0.05	12.0±1.50

3.3. Separation Performance of Membranes

The separation performance of the fabricated membranes was determined in terms of water flux, rejection, and anti-fouling properties. At least three measurements were made to for each performance indicator and the average of these values were reported.

Water flux and SA rejections of the fabricated membranes are shown in Figure 8. According to Figure 8, water flux values of pristine PVDF, PVDF/ZnO, PVDF/ZnO/PDA, and PVDF/PDA membranes were determined as 45 L/m^{2}h, 46 L/m^{2}h, 49 L/m^{2}h, and 32 L/m^{2}h, respectively. This result showed that modification of PVDF matrix with nanoparticles resulted in no significant change

Open Journal of Nano
ISSN: 2147-0081
(2022) 7–2
Research Article

in water flux, whereas surface coating caused a reduction in the flux. This was supported by observing a significant amount of ZnO and PDA clusters on the surface of the PVDF/ZnO (Fig. 3b) and PVDF/PDA (Fig. 3d) membrane in the SEM analysis, respectively, and the porosity results.

The SA removal of pristine PVDF membrane increased from 93% to 95% and 97%, with the addition of ZnO and ZnO/PDA fillers to the membrane matrix, respectively, which was attributed to the improved hydrophilicity of the matrix. The increase in hydrophilicity with the addition of fillers reduced the interaction between SA and the membrane surface, preventing the penetration of contaminant molecules through modified membranes during SA filtration [57, 58].

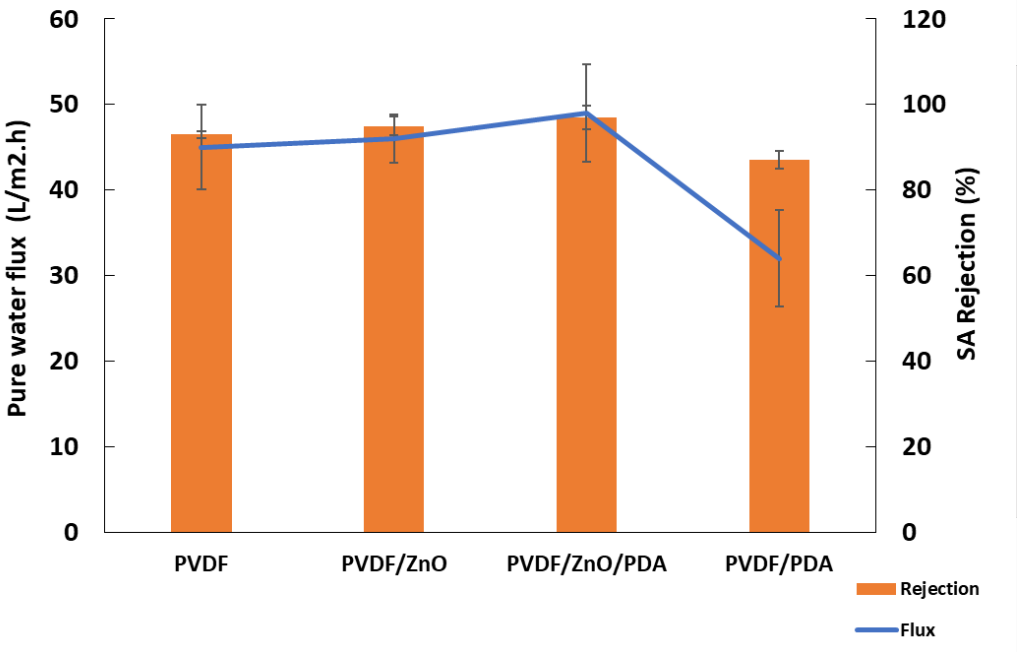

Figure 8. Water flux and SA rejections of the fabricated membranes.

The compaction behavior of the nanocomposite membranes in comparison to that of pristine PVDF membranes were investigated by measuring the water flux values at varying transmembrane pressures. As seen in Figure 9, water flux of all fabricated membranes increased with the applied transmembrane pressure. Even though the water flux of PVDF, PVDF/ZnO, and PVDF/ZnO/PDA membranes increased linearly with TMP until 0.15 MPa and 0.20 MPa, respectively, deviations from linearity were observed for all three membranes due to the pore deformation. However, the water flux values of the PVDF/ZnO/PDA membrane remained linear until the highest applied pressure, which revealed that with the addition of ZnO/PDA powders to the membrane matrix, the pore integrity was maintained even at high transmembrane pressures as a result of improvement in mechanical properties. The results agree well the mechanical properties given in Table 3.

Open Journal of Nano
ISSN: 2147-0081
(2022) 7–2
Research Article

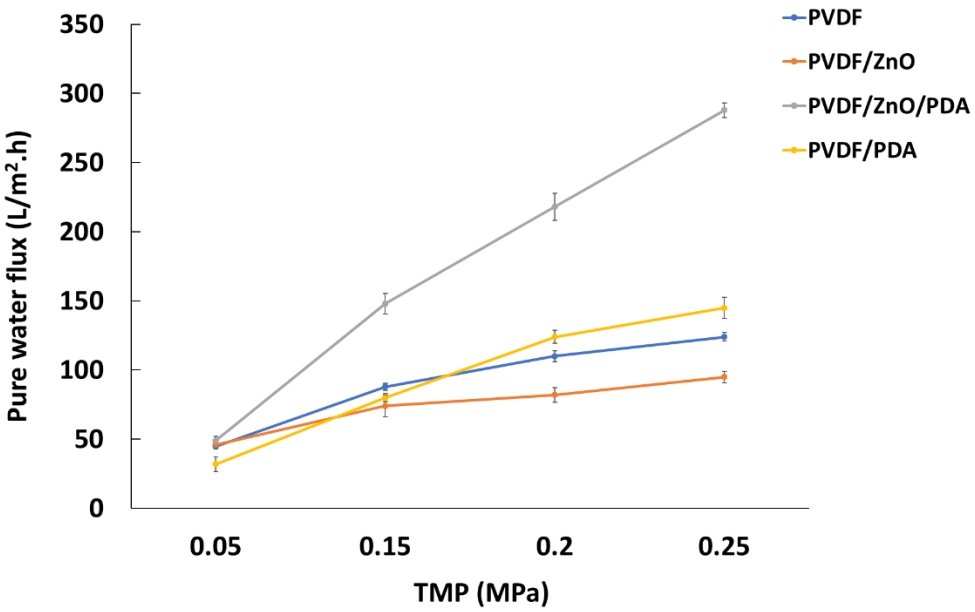

Figure 9. Variation of water flux with transmembrane pressure.

The anti-fouling properties of the fabricated membranes determined in terms of FRR and resistance values are shown in Figures 10 and 11, respectively. The FRR of the pristine PVDF membrane was as low as 51% due to the extremely hydrophobic nature of PVDF. Modification of membrane matrix with ZnO, PVDF/ZnO, and PDA provided an increase in FRR values to 57%, 92%, and 70%, respectively. The negatively charged groups (-OH) in ZnO/PDA nanoparticles repel the negative ions in the SA foulant solution mitigating the adsorption of the particles onto the membrane surface and internal pores, and therefore the anti-fouling properties were enhanced markedly [59]. In addition, the hydration layer induced on the membrane surface due to the presence of hydrophilic fillers would inhibit SA molecules from attaching to the membrane surface [60]. The FRR value of the PVDF/PDA membrane was not as high as PVDF/ZnO/PDA membrane due to the uneven distribution of PDA fillers in the matrix.

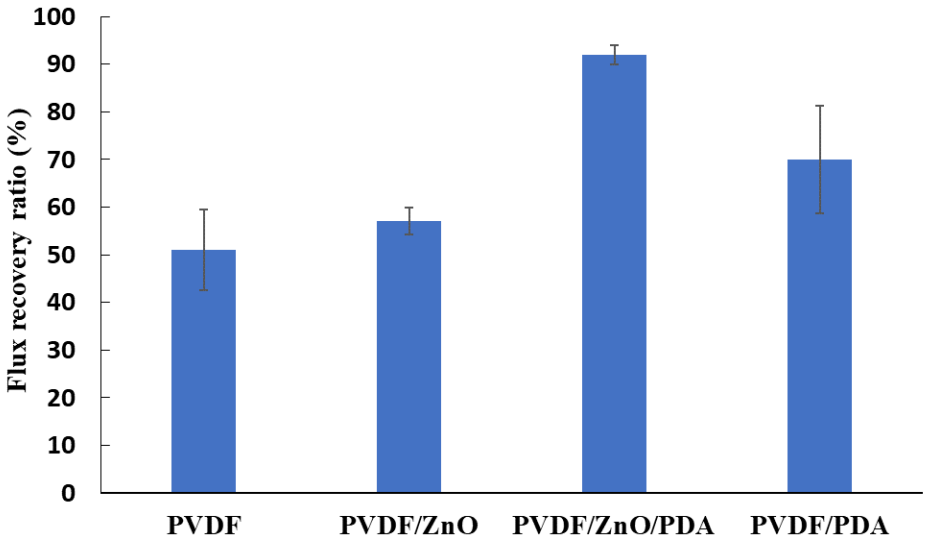

Figure 10. FRR values of the fabricated membranes after SA fouling.

According to Figure 11, the total fouling resistance of the ZnO/PDA membrane decreased compared to that of the pure PVDF membrane. The irreversible resistance of the pristine PVDF membrane (12.75×10^8 m^{-1}) decreased to 10.05×10^8 m^{-1} and 0.70×10^8 m^{-1} with the addition of ZnO and ZnO/PDA fillers into the matrix, respectively. This result confirmed that the improvement of

Open Journal of Nano
ISSN: 2147-0081
(2022) 7–2
Research Article

membrane hydrophilicity with the addition of ZnO/PDA powders reduced the interaction between SA and membrane surface, which in turn avoided the permanent fouling [57, 58]. Non-uniform distribution of PDA coating layer on the surface led to a comparatively higher internal membrane resistance with regards to pristine PVDF membrane and yet no significant improvement was demonstrated in reversible and irreversible resistances.

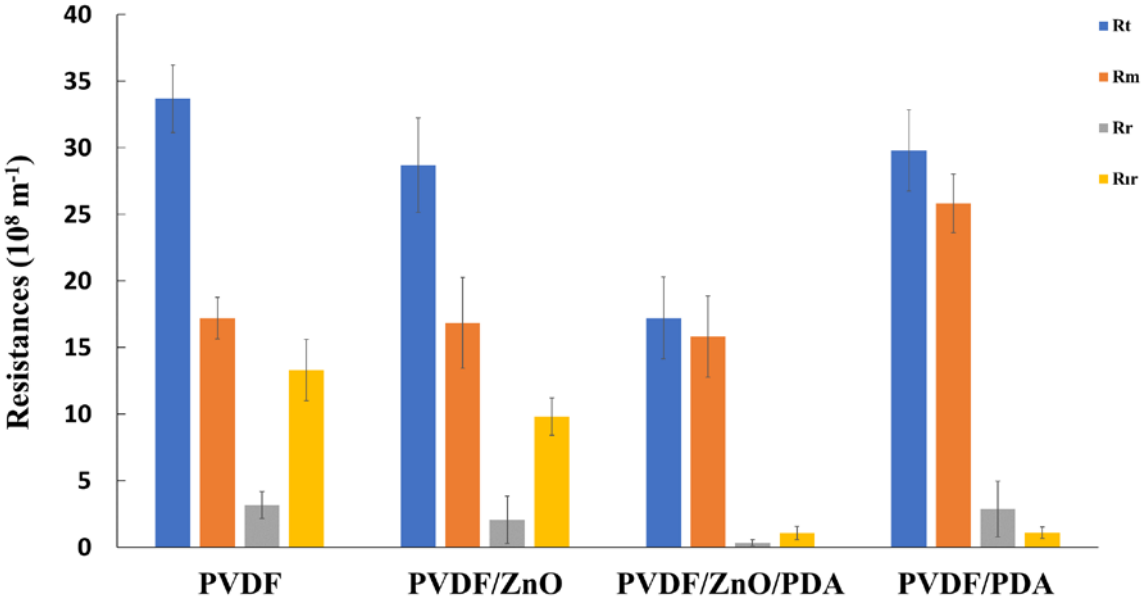

Figure 11. Filtration resistances of the fabricated membranes during SA fouling.

3.4. Lead Removal Efficiency

Since the pore sizes of the ultrafiltration membranes were not appropriate to separate Pb^{+2} ions with high efficiency, chitosan as the chelating agent was used for binding the metal to form macromolecular complexes (Figure 1). The lead-chitosan removal efficiencies of the fabricated membranes were investigated for a constant Pb^{+2} concentration of 10 ppm and pH value of 9.0 for different lead/chitosan ratios of 1:50 and 1:100 by mass. The results are given in Figure 12.

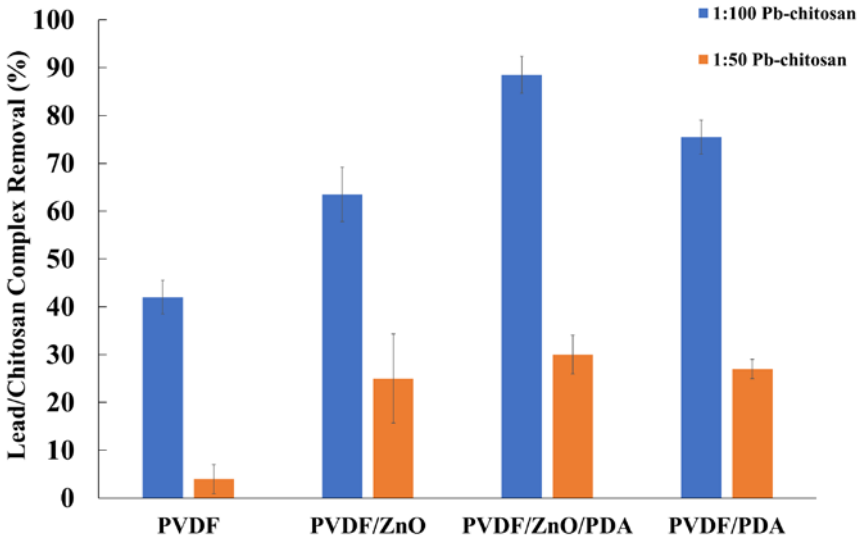

Figure 12. Lead-chitosan complex removal performance of membranes at different Pb/chitosan ratios (pH:9).

Chitosan, which is a cationic polyelectrolyte, is soluble in aqueous acidic media, and chelates metal ions. The formation of the metal-chitosan complex occurs primarily through the amino groups of chitosan, which act as ligands [61]. The interaction of metal ions with -OH and -NH_2 connects one or more chitosan chains. The complex structure formed has a larger diameter than the membrane pores allowing the Pb^{+2} ions to be retained by the membrane [62, 63]. The main parameters affecting on complexation of target metal with polymer are metal and polymer type, loading (the ratio of metal to polymer), pH, and existence of other metal ions in the solution [63]. As seen in Figure 12, lead-chitosan complex removal efficiency of pristine PVDF membrane increased as a result of the addition of different fillers into the pristine membrane matrix. Moreover, doubling the concentration of chitosan led to a marked increase in the lead-chitosan removal efficiency from aqueous solutions in the case of all fabricated membranes. The lead-chitosan complex removal performances of pristine PVDF, PVDF/ZnO, PVDF/ZnO/PDA, and PVDF/PDA membranes were determined as 42%, 63.5%, 88.5%, and 75.5%, respectively for a lead-chitosan ratio of 1:100. Among the fabricated membranes, PVDF/ZnO/PDA membrane exhibited the highest lead-chitosan complex removal efficiency, which was probably due to the combined effects of uniform dispersion of ZnO/PDA nanoparticles in the membrane matrix, especially on the surface and relatively small pore size distribution of the PVDF/ZnO/PDA membrane.

4. Conclusions

In the present study, PVDF-based nanocomposite flat-sheet membranes were developed by adding certain amounts of ZnO and ZnO/PDA powders to the membrane matrix and coating the membrane surface with PDA. The separation performance of the membranes were investigated in terms of water flux, sodium alginate (SA) rejection, and antifouling properties in comparison to pristine PVDF membrane. Moreover, lead removal efficiencies of the membranes from aqueous solutions with polymer-enhanced ultrafiltration method was investigated using chitosan as a chelating agent. The SEM images exhibited remarkable changes in pristine PVDF membrane morphology with higher connectivity among channels due to the presence of ZnO/PDA powders, indicating a uniform dispersion of the fillers as well as strong interaction with the polymer chains. As a result, bulk properties such as thermal stability and mechanical strength were enhanced substantially. Even though there was no significant improvement in water permeability of the pristine membrane, SA rejection increased from 93% to 97%, and a marked enhancement of 80% was obtained for FRR value with the addition of 0.5% ZnO/PDA fillers into the membrane matrix. Moreover, PVDF/ZnO/PDA membrane provided the highest lead-chitosan complex removal efficiency of 88.5% from aqueous solutions for a Pb-chitosan ratio of 1:100, which was probably due to the combined effects of uniform ZnO/PDA dispersion in the matrix, and comparatively smaller pore size distribution of the membrane structure.

Peer-review: Externally peer - reviewed.

Conflict of Interest: No conflict of interest was declared by the authors. This paper has been presented at the ICENTE'21 (International Conference on Engineering Technologies) held in Konya (Turkey), November 18-20, 2021.

Financial Disclosure: The authors declared that this study has received no financial support.

References

[1] Hosseini, S. M., Alibakhshi, H., Jashni, E., Parvizian, F., Shen, J. N., Taheri, M., & Rafiei, N. (2020). A novel layer-by-layer heterogeneous cation Exchange membrane for heavy metal ions removal from water. *Journal of hazardous materials*, 381, 120884.

[2] Naz, S., Rasheed, T., Naqvi, S. T. R., Hussain, D., Fatima, B., ul Haq, M. N., & Ibrahim, M. (2020). Polyvinylpropyllidone decorated manganese ferrite-based cues for the efficient removal of heavy metals ions from wastewater. *Physica B: Condensed Matter*, 599, 412559.

[3] Zhou, Q., Yang, N., Li, Y., Ren, B., Ding, X., Bian, H., & Yao, X. (2020). Total concentrations and sources of heavy metal pollution in the global river and lake water bodies from 1972 to 2017. *Global Ecology and Conservation*, 22, e00925.

[4] Zhou, D., Zhu, L., Fu, Y., Zhu, M., & Xue, L. (2015). Development of lower-cost seawater desalination processes using nanofiltration technologies. *Desalination*, 376, 109- 116.

[5] Fasaee, M. A. K., Berglund, E., Pieper, K. J., Ling, E., Benham, B., & Edwards, M. (2021). Developing a framework for classifying water lead levels at private drinking water systems: A Bayesian Belief Network approach. *Water Research*,189, 116641.

[6] Fang, X., Li, J., Li, X., Pan, S., Zhang, X., Sun, X., ... & Wang, L. (2017). Internal pore decoration with polydopamine nanoparticle on polymeric ultrafiltration membrane for enhanced heavy metal removal. *Chemical Engineering Journal*, 314, 38-49.

[7] Hajdu, I., Bodnár, M., Csikós, Z., Wei, S., Daróczi, L., Kovács, B., ... & Borbély, J. (2012). Combined nano-membrane technology for removal of lead ions. *Journal of Membrane Science*, *409*, 44-53.

[8] Sheng, P. X., Ting, Y. P., Chen, J. P., & Hong, L. (2004). Sorption of lead, copper, cadmium, zinc, and nickel by marine algal biomass: characterization of biosorptive capacity and investigation of mechanisms. *Journal of colloid and interface science*, *275*(1), 131-141.

[9] He, J., Xiong, D., Zhou, P., Xiao, X., Ni, F., Deng, S., & Luo, L. (2020). A novel homogenous in-situ generated ferrihydrite nanoparticles/polyethersulfone composite membrane for removal of lead from water: Development, characterization, performance, and mechanism. *Chemical Engineering Journal*, 393, 124696.

[10] Wang, K., Abdalla, A. A., Khaleel, M. A., Hilal, N. Khraisheh, M. K. (2017). Mechanical Properties of Water Desalination and Wastewater Treatment Membranes. *Desalination*. 401, 190-205.

[11] Xu, W., Sun, X., Huang, M., Pan, X., Huang, X., & Zhuang, H. (2020). Novel covalent organic framework/PVDF ultrafiltration membranes with antifouling and lead removal performance. *Journal of Environmental Management*, 269, 110758.

[12] Ali, H., & Khan, E. (2019). Bioaccumulation of Cr, Ni, Cd, and Pb in the economically important freshwater fish Schizothorax plagiostomus from three rivers of Malakand Division, Pakistan: risk assessment for human health. *Bulletin of environmental contamination and toxicology*, 102(1), 77-83.

[13] Mulder, M., & Mulder, J. (1996). *Basic principles of membrane technology*. Springer Science & Business Media.

[14] Aslan, M. (2016). Membran Teknolojileri. *T.C. Çevre ve Şehircilik Bakanlığı*. 57-218.

[15] Gebru, K. A., & Das, C. (2018). Removal of chromium (VI) ions from aqueous solutions using amine impregnated TiO_2 nanoparticles modified cellulose acetate membranes. *Chemosphere*, *191*, 673-684.

[16] Ursino, C., Castro-Muñoz, R., Drioli, E., Gzara, L., Albeirutty, M. H., & Figoli, A. (2018). Progress of nanocomposite membranes for water treatment. *Membranes*, *8*(2), 18.

[17] Bai, H., Wang, X., Zhou, Y., & Zhang, L. (2012). Preparation and characterization of poly (vinylidene fluoride) composite membranes blended with nano-crystalline cellulose. *Progress in Natural Science: Materials International*, *22*(3), 250-257.

[18] Hong, J., & He, Y. (2012). Effects of nano-sized zinc oxide on the performance of PVDF microfiltration membranes. *Desalination, 302*, 71-79.

[19] Shi, H., He, Y., Pan, Y., Di, H., Zeng, G., Zhang, L., & Zhang, C. (2016). A modified mussel-inspired method to fabricate TiO_2 decorated superhydrophobic PVDF membrane for oil/water separation. *Journal of Membrane Science, 506*, 60-70.

[20] Zhang, Q., Cui, Z., & Li, W. (2020). High permeability poly (vinylidene fluoride) ultrafiltration membrane doped with polydopamine modified TiO_2 nanoparticles. *Chinese Journal of Chemical Engineering, 28(12),* 3152-3158.

[21] Liebscher, J. (2019). Chemistry of polydopamine–scope, variation, and limitation. *European Journal of Organic Chemistry, 2019*(31-32), 4976-4994.

[22] Tavakoli, S., Kharaziha, M., & Nemati, S. (2021). Polydopamine coated ZnO rod-shaped nanoparticles with noticeable biocompatibility, hemostatic and antibacterial activity. *Nanostructures & Nano-Objects,* 25, 100639.

[23] Trivunac, K., & Stevanovic, S. (2006). Removal of heavy metal ions from water by complexation-assisted ultrafiltration. *Chemosphere,* 64(3), 486-491.

[24] Juang, R. S., & Shiau, R. C. (2000). Metal removal from aqueous solutions using chitosan-enhanced membrane filtration. *Journal of membrane science,* 165(2), 159-167.

[25] Petrov, S., & Nenov, V. (2004). Removal and recovery of copper from wastewater by a complexation-ultrafiltration process. *Desalination,* 162, 201-209.

[26] Müslehiddinoğlu, J., Uludağ, Y., Özbelge, H. Ö., & Yilmaz, L. (1998). Effect of operating parameters on selective separation of heavy metals from binary mixtures via polymer enhanced ultrafiltration. *Journal of Membrane Science,* 140(2), 251-266.

[27] Vieira, M., Tavares, C. R., Bergamasco, R., & Petrus, J. C. C. (2001). Application of ultrafiltration-complexation process for metal removal from pulp and paper industry wastewater. *Journal of Membrane Science,* 194(2), 273-276.

[28] Zhang, Y. F., & Xu, Z. L. (2003). Study on the treatment of industrial wastewater containing Pb2+ ion using a coupling process of polymer complexation-ultrafiltration. *Separation Science and Technology,* 38(7), 1585-1596.

[29] Llorens, J., Pujola, M., & Sabaté, J. (2004). Separation of cadmium from aqueous streams by polymer enhanced ultrafiltration: a two-phase model for complexation binding. *Journal of Membrane Science, 239*(2), 173-181.

[30] Freire, E., Bianchi, O., Monteiro, E. E., Nunes, R. C. R., & Forte, M. C. (2009). Processability of PVDF/PMMA blends studied by torque rheometry. *Materials Science and Engineering:* C, 29(2), 657-661.

[31] Ma, F. F., Zhang, N., Wei, X., Yang, J. H., Wang, Y., & Zhou, Z. W. (2017). Blend-electrospun poly (vinylidene fluoride)/polydopamine membranes: self-polymerization of dopamine and the excellent adsorption/separation abilities. *Journal of Materials Chemistry A, 5(27),* 14430-14443.

[32] Gu, X., Zhang, Y., Sun, H., Song, X., Fu, C., & Dong, P. (2015). Mussel-inspired polydopamine coated iron oxide nanoparticles for biomedical application. *Journal of Nanomaterials,* Article ID 154592.

[33] Demirel, E., Zhang, B., Papakyriakou, M., Xia, S., & Chen, Y. (2017). Fe2O3 nanocomposite PVC membrane with enhanced properties and separation performance. *Journal of membrane science, 529,* 170-184.

[34] Wu, G., Gan, S., Cui, L., & Xu, Y. (2008). Preparation and characterization of PES/TiO2 composite membranes. *Applied Surface Science*, *254*(21), 7080-7086.

[35] Vatanpour, V., Madaeni, S. S., Moradian, R., Zinadini, S., & Astinchap, B. (2012). Novel antifouling nanofiltration polyethersulfone membrane fabricated from embedding TiO2 coated multiwalled carbon nanotubes. *Separation and purification technology*, *90*, 69-82.

[36] Mahmoudi, C., Demirel, E., & Chen, Y. (2020). Investigation of characteristics and performance of polyvinyl chloride ultrafiltration membranes modified with silica-oriented multi-walled carbon nanotubes. *Journal of Applied Polymer Science*, *137*(45), 49397.

[37] Juang, R. S., & Chiou, C. H. (2000). Ultrafiltration rejection of dissolved ions using various weakly basic water-soluble polymers. *Journal of Membrane Science*, 177(1-2), 207-214.

[38] Zhang, X., Wang, Y., Liu, Y., Xu, J., Han, Y., & Xu, X. (2014). Preparation, performances of PVDF/ZnO hybrid membranes and their applications in the removal of copper ions. *Applied Surface Science*, 316, 333-340.

[39] Fedorenko, V., Viter, R., Mrówczyński, R., Damberga, D., Coy, E., & Iatsunskyi, I. (2020). Synthesis and photoluminescence properties of hybrid 1D core–shell structured nanocomposites based on ZnO/polydopamine. *RSC Advances, 10(50),* 29751-29758.

[40] Muhammad, W., Ullah, N., Haroon, M., & Abbasi, B. H. (2019). Optical, morphological, and biological analysis of zinc oxide nanoparticles (ZnO NPs) using Papaver somniferum L. *RSC Advances*, 9(51), 29541-29548.

[41] Meng, R., Chen, Y., Zhang, X., Dong, X., Ma, H., & Wang, G. (2017). Synthesis of a hydrophilic α-sulfur/PDA composite as a metal-free photocatalyst with enhanced photocatalytic performance under visible light. *Journal of Macromolecular Science-Pure and Applied Chemistry*, *54*(5), 334-338.

[42] Popa, A., Toloman, D., Stan, M., Stefan, M., Radu, T., Vlad, G., & Pana, O. (2021). Tailoring the RhB removal rate by modifying the PVDF membrane surface through ZnO particles deposition. *Journal of Inorganic and Organometallic Polymers and Materials*, *31*(4), 1642-1652.

[43] Syawaliah, S., Arahman, N., Riza, M., & Mulyati, S. (2018). The influences of polydopamine immersion time on characteristics and performance of polyvinylidene fluoride ultrafiltration membrane. In *MATEC Web of Conferences* (Vol. 197, p. 09007). EDP Sciences.

[44] Guclu, S., Erkoc-Ilter, S., Koseoglu-Imer, D. Y., Unal, S., Menceloglu, Y. Z., Ozturk, I., & Koyuncu, I. (2019). Interfacially polymerized thin-film composite membranes: Impact of support layer pore size on active layer polymerization and seawater desalination performance. *Separation and Purification Technology*, 212, 438-448.

[45] Muchtar, S., Wahab, M. Y., Fang, L. F., Jeon, S., Rajabzadeh, S., Takagi, R., & Matsuyama, H. (2019). Polydopamine-coated poly (vinylidene fluoride) membranes with high ultraviolet resistance and antifouling properties for a photocatalytic membrane reactor. *Journal of Applied Polymer Science*, *136*(14), 47312.

[46] Li, N., Tian, Y., Zhang, J., Sun, Z., Zhao, J., Zhang, J., & Zuo, W. (2017). Precisely controlled modification of PVDF membranes with 3D TiO_2/ZnO nanolayer: enhanced anti-fouling performance by changing hydrophilicity and photocatalysis under visible light irradiation. *Journal of Membrane Science*, 528, 359-368.

[47] Meng, R., Chen, Y., Zhang, X., Dong, X., Ma, H., & Wang, G. (2017). Synthesis of a hydrophilic α-sulfur/PDA composite as a metal-free photocatalyst with enhanced

photocatalytic performance under visible light. *Journal of Macromolecular Science, Part A*, 54(5), 334-338.

[48] Moazeni, N., Sadrjahani, M., Merati, A. A., Latifi, M., & Rouhani, S. (2019). Effect of stimuli-responsive polydiacetylene on the crystallization and mechanical properties of PVDF nanofibers. *Polymer Bulletin*, *77*(17) 1-16.

[49] Li, J. H., Ni, X. X., Zhang, D. B., Zheng, H., Wang, J. B., & Zhang, Q. Q. (2018). Engineering self-driven PVDF/PDA hybrid membranes based on membrane micro-reactor effect to achieve super-hydrophilicity, excellent antifouling properties, and hemocompatibility. *Applied Surface Science*, 444, 672-690.

[50] Sorayani Bafqi, M. S., Bagherzadeh, R., & Latifi, M. (2015). Fabrication of composite PVDF-ZnO nanofiber mats by electrospinning for energy scavenging application with enhanced efficiency. *Journal of polymer research*, 22(7), 1-9.

[51] Radwan, A. B., Mohamed, A. M., Abdullah, A. M., & Al-Maadeed, M. A. (2016). Corrosion protection of electrospun PVDF–ZnO superhydrophobic coating. S*urface and Coatings Technology*, 289, 136-143.

[52] Spasova, M., Manolova, N., Markova, N., & Rashkov, I. (2017). Tuning the properties of PVDF or PVDF-HFP fibrous materials decorated with ZnO nanoparticles by applying electrospinning alone or in conjunction with electrospraying. *Fibers and Polymers*, 18(4), 649-657.

[53] Jiang, J. H., Zhu, L. P., Zhang, H. T., Zhu, B. K., & Xu, Y. Y. (2014). Improved hydrodynamic permeability and antifouling properties of poly (vinylidene fluoride) membranes using polydopamine nanoparticles as additives. *Journal of Membrane Science*, *457*, 73-81.

[54] Yan, L., Li, Y. S., Xiang, C. B., & Xianda, S. (2006). Effect of nano-sized Al_2O_3-particle addition on PVDF ultrafiltration membrane performance. *Journal of Membrane Science*, 276(1-2), 162-167.

[55] Wan, Y., Wu, Q., Wang, S., Zhang, S., & Hu, Z. (2007). Mechanical properties of porous polylactide/chitosan blend membranes. *Macromolecular Materials and Engineering, 292*, 598–607.

[56] Manawi, Y. M., Wang, K., Kochkodan, V., Johnson, D. J., Atieh, M. A., & Khraisheh, M. K. (2018). Engineering the surface and mechanical properties of water desalination membranes using ultralong carbon nanotubes. *Membranes*, *8*(4), 106.

[57] Breite, D., Went, M., Prager, A., & Schulze, A. (2015). Tailoring membrane surface charges: A novel study on electrostatic interactions during membrane fouling. *Polymers*, *7*(10), 2017–2030.

[58] Rana, D., & Matsuura, T. (2010). Surface modifications for antifouling membranes. *Chemical Reviews*, 110(4), 2448-2471.

[59] Lalia, B. S., Kochkodan, V., Hashaikeh, R., & Hilal, N. (2013). A review on membrane fabrication: Structure, properties, and performance relationship. *Desalination*, *326*, 77-95.

[60] Kumar, R., & Ismail, A. F. (2015). Fouling control on microfiltration/ultrafiltration membranes: Effects of morphology, hydrophilicity, and charge. *Journal of Applied Polymer Science, 132*(21), 42042.

[61] Krajewska, B. (2001). Diffusion of metal ions through gel chitosan membranes. *Reactive and Functional Polymers*, *47*(1), 37-47.

[62] Wang, X., Du, Y., Fan, L., Liu, H., & Hu, Y. (2005). Chitosan-metal complexes as antimicrobial agent: synthesis, characterization, and structure-activity study. *Polymer Bulletin*, *55*(1), 105-113.

[63] Garba, M. D., Usman, M., Mazumder, M. A. J., & Al-Ahmed, A. (2019). Complexing agents for metal removal using ultrafiltration membranes: *Environmental Chemistry Letters*, 1-14.